Raman Evidence for absence of Phase Transitions in Negative Differential Resistance thin film devices of Niobium Dioxide

Ali Fakih, Onkar Shinde, Johan Biscaras, Abhay Shukla

Raman Evidence for absence of Phase Transitions in Negative Differential Resistance thin film devices of Niobium Dioxide

Ali Fakih,[1] Onkar Shinde,[1] Johan Biscaras,[1,*] and Abhay Shukla[1,†]

[1]*Institut de Minéralogie, de Physique des Matériaux et de Cosmochimie, Sorbonne Université, UMR CNRS 7590, MNHN, 4 Place Jussieu, F-75005 Paris, France*

Abstract

We fabricate NbO_2 thin films and measure their transport properties in simple devices. These could be potential components of future memristor devices because of peculiar conductivity variations observed as a function of device current. We find that threshold switching effects observed in the voltage control regime are better viewed in the current controlled regime where they can be understood in terms of a negative differential resistance phenomenon. No electronic or structural phase change is observed in the NbO_2 thin films in this regime in the steady state, notably with in-situ Raman measurements. In particular, both crystalline and amorphous films remain insulating since their resistance always decreases with increase in temperature. However, a large decrease in resistivity corresponding to negative differential resistance is observed as current in the devices increases. Temperature is the parameter which induces this change in resistivity through thermal activation of carriers, confirming recent understanding of the phenomenon. Temperature changes are locally induced because of power dissipated by the current in the device and the intrinsically low thermal conductivity of NbO_2. This is confirmed by parameters extracted from simulation of the phenomenon with different transport models. However, the simplest thermal activation model accounts for the observations in non-nanometric devices without the need for invoking more complex models. Finally, pulsed current can be used to provoke a structural, amorphous to crystalline phase transition in amorphous samples through sudden local increase in temperature.

DOI: **PACS numbers:**

INTRODUCTION

Threshold switching in niobium oxides, in which the current abruptly increases at an onset voltage, has been reported as early as the 1960's [1]. This phenomenon has been observed not only in stoichiometric NbO_2 [2], but also in metal-rich nonstoichiometric phases of NbO_x [3–5]. However, different studies attribute this switching to different origins and to different underlying physical concepts behind the threshold switching mechanism. These include a thermally driven metal insulator transition originating in Joule heating [6–8], modifications in the electronic structure by an applied electric field [2, 9, 10], and more recently, current and temperature controlled negative differential resistance [11].

Most studies have concentrated on a measurement geometry that can be directly incorporated in devices. This often implies a thin layer film of NbO_x (typically few tens of nm), probed vertically across its thickness, with the device area limited laterally by the size of one of the contacts which can also be typically a few tens of nm. This means a very small NbO_2 volume in the device [11, 12]. Wang et al. [13] fabricated $Nb/NbO_2/TiN$ sandwich vertical devices and studied the response of NbO_2 to an applied electric field. They report unipolar threshold switching characteristics with repeatability up to hundreds of cycles and thermal stability up to 150°C. They suggested that hopping conduction was the dominant conduction process in the NbO_2 insulating state and a metal insulator transition occurred which was not thermally driven but due to changes in the electronic structure. Kumar et al. [11] also fabricated vertical NbO_2 sandwich devices. They studied the response of NbO_2 under the application of current and identified two domains where NbO_2 exhibits negative differential resistance (NDR), one at around 400K caused by Joule-heating-driven thermal runaway and the other at around 1000 K which is a hysteretic, temperature controlled metal insulator transition.

In this work we focus on questions concerning these phenomena in NbO_2. The role of the electric field, current and temperature in provoking these phenomena is studied as well as the eventual occurrence of structural changes or phase transitions which we investigate with in-situ Raman measurements.

MATERIALS AND METHODS

Unlike most NbO_2 or NbO_x devices which are used in such studies where a thin film is sandwiched between two conducting contacts, at least one of which is nanometric in size, ($Pt/TiN/NbO_x$ /W [14], Pt/NbO_2 /Pt [15], Nb/NbO_2 /TiN [9]) our thin films were deposited on an n-doped 280 μm thick silicon substrate Si $< 100 >$, or on a 500 μm thick soda-lime glass substrate [16]. The Si substrate acts as the bottom electrode and 50 nm of gold is deposited on the NbO_2 film as a top electrode. The as-deposited films are amorphous and can be transformed to the poly-crystalline form by annealing in vacuum (10^{-6} mbar $< p < 10^{-5}$ mbar) for 4 hrs at 600°C (here) or at a higher temperature. Figure 1 (a)and (b) show X-Ray diffraction and Raman spectra from a 130 nm thick poly-crystalline film on the Si substrate showing that it is single phase NbO_2 [13]. A 10x (or 50x) objective was used to focus a 532 nm wavelength laser beam into a 1 μm (or 0.7 μm) diameter spot on the sample with an incident power of 0.25 mW. The size of the micro-Raman incident beam makes it possible to precisely aim at the region between the contacts. For each Raman measurement at a given (I,V) couple, the current was gradually increased from zero to I and the corresponding steady state voltage V was obtained. The Raman measurement was then performed, the current was reduced to zero and the system was allowed to stabilize back to room temperature before the next (I,V) measurement. Thus there is no possibility of cumulative laser heating in the measurements. During a given Raman measurement no shift in the Raman peak of Si was observed and the minimal power of the incident beam ensures the absence of heating. The power dissipated per unit surface by the laser beam is of the order of a 100 $\mu W/\mu m^2$, much less than that due to the current. The films were contacted for transport measurements as explained below. In-situ Raman measurements were made with an Xplora micro-Raman spectrometer through the optical window of a cryostat. The sample was mounted in the cryostat and electrical measurements were made in vacuum with the simultaneous possibilities of Raman measurements and of heating the sample to 400 K.

The I-V curves were measured along the vertical direction in the thin film on the Si substrate, between a contact on the sample surface and the substrate (Figure 1 (c)). We note two principal features. Firstly we observe asymmetric-diode like characteristics depending on the polarity. In a 'forward-bias' regime, the device conducts, in a 'reverse-bias' regime it does not conduct until a threshold voltage is reached. This diode-like behavior is a consequence

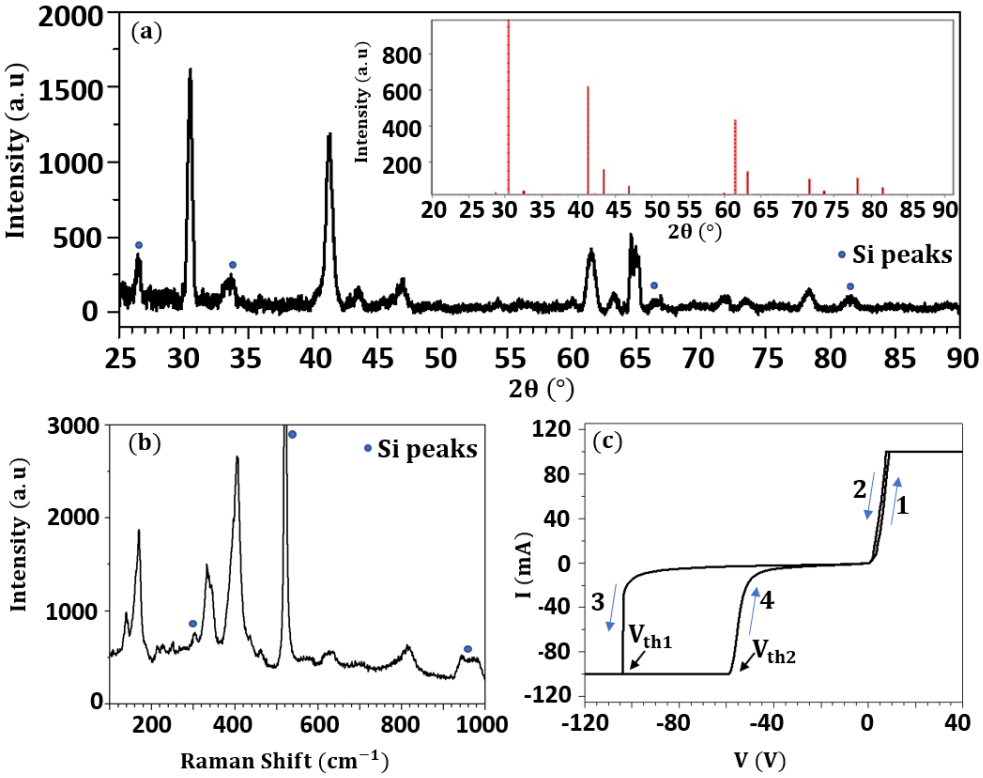

FIG. 1. Characterisation of NbO_2 thin films. a) X-ray diffraction spectrum of a 130 nm thick polycrystalline thin film on Si substrate. b) Raman spectrum of the same thin film c) I-V characteristics in a vertical geometry.

of the semiconductor-semiconductor Si-NbO_2 interface. The 'reverse-bias' regime, which is the one probed in all earlier work with a metal-NbO_2 interface contains the switching region which is often identified with a threshold voltage. One immediate conclusion is that this threshold voltage does not correspond to a Zener-like regime since it depends on the history

of the I-V cycle, ($V_{th_1} \neq V_{th_2}$, Figure 1 (c)). From systematic studies, we conclude that the threshold voltage is also dependent on contact geometry and shifts to lower voltages as the temperature increases and most importantly it is instrument related, depending on the compliance value of the current in voltage dependent measurements. This is easily resolved by making the measurements with a current source. Also, to avoid asymmetric diode-like behavior in the vertical measurements where one contact is NbO_2/Au and the other is NbO_2/Si, we switch to lateral measurements between two gold contacts on the sample surface (Figure 2). Three samples were used in the following experiments, both amorphous and poly-crystalline NbO_2 thin film on Si $< 100 >$ substrates and a poly-crystalline NbO_2 thin film on soda lime glass substrate. As shown in Figure 2 (b), contacts on the surface of these samples were either extended and obtained by gold evaporation using a stencil mask (Si substrates) or point contacts obtained by wire bonding 25 micron thick wire directly on the sample surface (glass substrate).

In Figure 2 (a), the measurements in lateral geometry between two contacts on the sample surface for thin films on both glass and Si substrates are shown only for the positive I-V quadrant as they no more exhibit the assymetric diode-like behavior seen earlier in the vertical geometry on the thin films on Si substrates. Furthermore, the current dependent measurements do not show an artificial threshold behavior, but clearly exhibit a negative differential resistance regime of the S-type. Note that the measurements have been symmetrised with respect to current direction to correct for deviations due to sample and contact geometry. The current is two orders of magnitude higher for the thin film on the Si substrate (left panel) with respect to the one on the glass substrate (right panel). Simulations taking into account the resistivity of NbO_2 (amorphous or poly-crystalline) with respect to both glass and Si show that in the case of the glass substrate, the current resides essentially in the NbO_2 film, between the two point contacts. In the case of the Si substrate the current penetrates the NbO_2 film vertically from the extended contacts to the Si substrate and then flows laterally between the two contacts, in the substrate. As shown schematically in Figure 2 (c), the current is much higher in the samples on the Si substrate because of the extended contacts but probably very similar in terms of current density, given the similar behavior for the negative differential resistance. We also investigate the occurrence of the clear hysterisis in our measurements in which the current is swept and the corresponding voltage measured. Some earlier works also find hysterisis in the I-V characteristics [9, 12] while it has not been

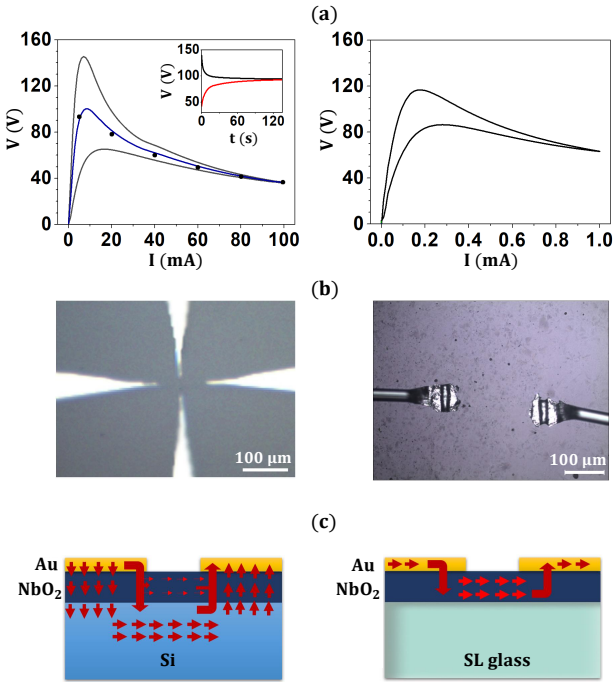

FIG. 2. Current controlled measurements in lateral geometry (a) Characteristics of poly-crystalline thin films on Si (left) and glass (right) substrates. In the left panel, the solid black line represents the measured hysteretic cycle with the automated 'fast' measurement. The solid blue line represents the average over the cycle. The black dots show the steady state voltage obtained after waiting for several minutes with the current fixed at certain values. The inset shows the relaxation of the voltage during the interruption at 5 mA during the forward sweep (black) and the backward sweep (red). The current flowing through the sample on the Si substrate (left) is two orders of magnitude larger than the current flowing through the sample on the glass substrate (right). (b) Pictures of lateral contact geometry for samples on silicon substrate (left) and glass substrate (right). (c) Schematics of the current flow through the corresponding devices.

observed in measurements of NbO_2 nanometric devices. It was found by stopping the current sweep at fixed values that the corresponding voltage varied as a function of time before attaining a steady state value in a few minutes (Figure 2 (a)). The steady state curve is nicely approximated by the average of the hysteretic I-V measurement as shown by the few directly measured steady state values which fall on the average curve. The reason for the

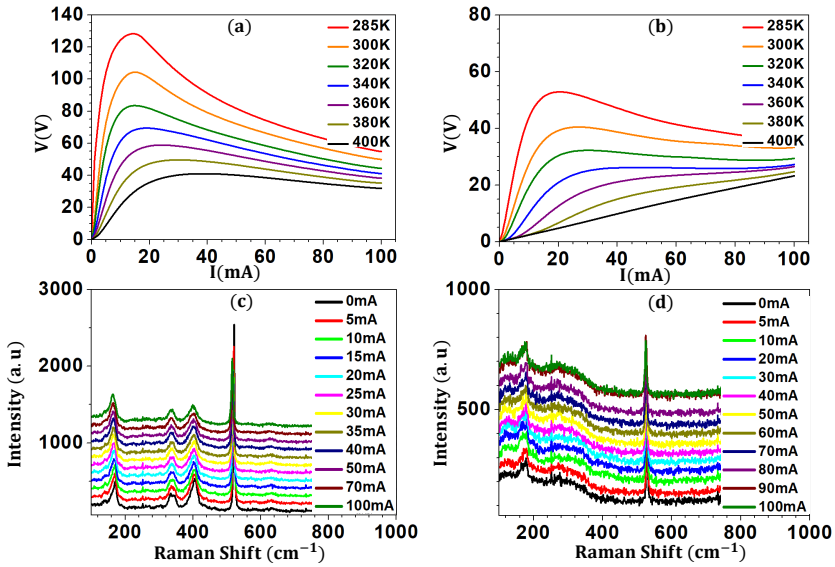

FIG. 3. Effect of temperature on the V(I) curves of a) crystalline and b) amorphous NbO_2 films on Si substrates. For both samples as the temperature increases the low current resistance decreases as well as the negative differential resistance effect. In the amorphous sample the differential resistance vanishes at 400 K. Raman spectrum of a) crystalline and b) amorphous NbO_2 films on Si substrates at diffrent values of the current. No variation is observed except for a small expected red-shift of the peaks due to temperature variation.

hysteresis is assumed to be the time required to attain thermal equilibrium in the effective sample volume after Joule heating, a hypothesis which is reinforced by diminishing hysteresis if the whole sample is progressively heated from outside. In the following we discuss such averaged, symmetrised I-V curves in the current-control regime for the different samples.

RESULTS AND DISCUSSION

Since heat dissipated by current flow in the sample causes changes in the sample conductivity, one would like to know how NDR is influenced by increasing the sample temperature. To investigate this we measure the NDR curves for both the amorphous and crystalline films on Si substrates. The amorphous film has lower resistivity than the poly-crystalline film. For both samples, as the temperature increases from 285 K to 400 K, resistance decreases at low current as shown in Figure 3 (a) and (b). A similar behavior is found in the current controlled negative differential resistance of $Co_2FeO_2BO_3$ and $Fe_3O_2BO_3$ [17].

In Figure 3 (b), for the amorphous sample, we see that the NDR part of the curve progressively disappears and that at 400 K the relation between V and I is linear with a constant ohmic resistance. The poly-crystalline sample in Figure 3 (a) shows the same trend, but 400 K (the maximum temperature attained in our measuring system) is not enough to get rid of the NDR regime. However, one can estimate by comparison with the amorphous sample that a temperature between 500 and 600 K should suffice to suppress the NDR regime in this sample. To investigate the eventual involvement of a phase transition in the observed NDR behavior we measured Raman spectra of both samples as a function of temperature and at different points of the NDR cycle, with the micro Raman beam focussed between the contacts of the device. Figure 3 (c) and (d) show the Raman spectra measured in-situ at the steady state value of the indicated current for the polycrystalline and the amorphous samples respectively. No change in the Raman spectra are observed except those related to the expected small red-shift in Raman frequencies as temperature increases. The sharp peak at 520 cm^{-1} is from the Si substrate and its red-shift with increasing temperature can be used to estimate the sample temperature as will be shown below. We conclude that temperature induced conductivity change is the key phenomenon for the comprehension of NDR in NbO_2 and that no phase or structural transition is involved.

Threshold switching and commutation between two states or phases are often dynamic phenomena where energy deposited in a short time could generate phase transitions. We subjected our devices to current pulses to eventually observe such changes through Raman spectroscopy. Current pulses with an amplitude of 100 mA pulses and a period of 10 ms (see right inset of Figure 4) were applied to devices of both crystalline and amorphous samples. On the crystalline sample no changes were observed optically or in the Raman spectra after 50 pulses. On the other hand after a sequence of 10 pulses the amorphous sample showed a visual change corresponding to the current path. The left inset of Figure 4 shows the central device area of an amorphous sample after pulsing. Tracks a few microns wide appear between different sets of contacts where the pulsed current is passed. Raman spectra before pulsing and in the non-contrasted region after pulsing correspond to amorphous NbO_2. The appearance of characteristic NbO_2 Raman peaks in the region of the current tracks (Figure 4) after pulsing indicates crystallization of NbO_2 through local heating to at least 550 °C. It also validates the use of micro-Raman spectroscopy in the steady state NDR regime where no phase changes were found.

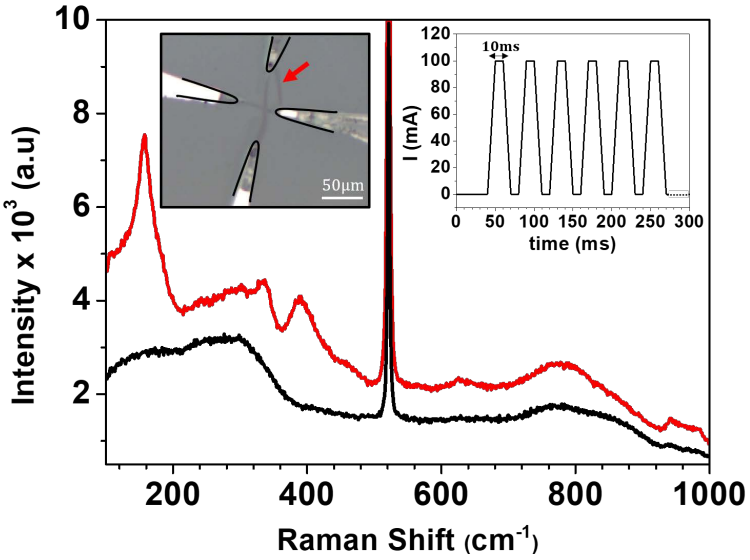

FIG. 4. Crystallization of an amorphous thin film after passing of pulsed current. The right inset shows the pulse structure. The left inset shows the central device area after pulsing. The contacts suffer damage due to pulsing and have been outlined for clarity. Tracks (indicated by a red arrow) a few microns wide appear between different sets of contacts where the pulsed current is passed. Raman spectra before pulsing or in the non-contrasted region after pulsing (black line), correspond to amorphous NbO_2. The appearance of characteristic NbO_2 Raman peaks for spectra taken in the region of the current tracks after pulsing (red line) indicates heat induced crystallization.

The increase of the current in a sample means that the dissipated power increases causing an increase in temperature. This increase in the temperature generates charge carriers causing NDR. The increase in conductivity with temperature for a semiconducting material can be simply written using thermal activation across a characteristic activation energy as:

$$\sigma = \sigma_0 \exp\left(-\frac{E_a}{k_B T}\right) \tag{1}$$

where σ_0 is the extrapolated zero temperature conductivity, E_a is the activation energy and k_B is the Boltzmann constant.

In a nanometric sized device, the electric field can be substantial because of the nanometric distances over which the potential is applied. In this case, when one takes the electric field effect on the conduction mechanism into account, the Poole-Frenkel conduction mechanism

modifies the conductivity as below [18, 19]:

$$\sigma = \sigma_0 \exp\left(\frac{-E_a + q\sqrt{qE/(\pi\epsilon)}}{k_{\mathrm{B}}T}\right) \tag{2}$$

where E is the applied electric field, q is the elementary charge, and $\epsilon = \epsilon_0\epsilon_i$ is the high frequency permittivity.

While the original Poole-Frenkel model is one-dimensional, a 3D version has been derived as below [20, 21]:

$$\sigma = \sigma_0 e^{-\frac{E_a}{k_{\mathrm{B}}T}}\left[\frac{1}{2} + \left(\frac{k_{\mathrm{B}}T}{q\sqrt{qE/(\pi\epsilon)}}\right)^2\left(1 + \left(\frac{q\sqrt{qE/(\pi\epsilon)}}{ak_{\mathrm{B}}T} - 1\right)e^{\frac{q\sqrt{qE/(\pi\epsilon)}}{ak_{\mathrm{B}}T}}\right)\right] \tag{3}$$

The parameter a in the Poole-Frenkel exponential term is equal to 1 in the standard Poole-Frenkel and 2 in the 'modified' Schottky version. This equation has been used first in [22] with $a = 2$, and later in [11] with $a = 1$.

In all the above models, the dynamic equation for the temperature (which is the state variable) is Newton's law of cooling:

$$\frac{\mathrm{d}T}{\mathrm{d}t} = \frac{I.V}{C_{th}} - \frac{T - T_{\mathrm{amb}}}{C_{th}R_{th}(T)} \tag{4}$$

where T_{amb} is the ambient temperature, C_{th} and R_{th} are the effective thermal capacitance and thermal resistance respectively. In the static limit where $\frac{\mathrm{dT}}{\mathrm{dt}} = 0$ equation (4) becomes $T = T_{\mathrm{amb}} + R_{th}IV$. The static limit is justified in our case as we are fitting the static non-hysteretic curves.

We chose the data from the polycrystalline film on the glass substrate for fitting with the models discussed above (thermal activation, standard Poole-Frenkel, modified Poole-Frenkel with a =1 or 2). Figure 5 (a) shows the measured V(I) and the best fits with the various models. Figure 5(b) shows the resulting local temperature extracted. This can be compared with the measured temperature (using the Si Raman peak) shown in 5(c), with a fit corresponding to the dynamic equation for the temperature given by Newton's law of cooling. The calibration of the temperature with the Si peak red-shift is from an

Physical quantity	**Symbol**	**Value**	**Unit**
Activation energy	E_a	0.269	eV
Effective length	d	40	µm
Cross-section area	A	1.32×10^{-11}	m^2
High frequency dielectric constant	ϵ_r	45 [23]	
Conductivity constant	σ_0	12100*	$S.m^{-1}$
Thermal resistance	R_{th}	1.6×10^4	$K.W^{-1}$

TABLE I. List of parameters used in the conduction models for fitting the experimental V(I) curve. *The fitting parameter σ_0 for the Poole-Frenkel model with $a = 2$ is multiplied by a factor of 8/5[22].

earlier measurement. The measured temperature is lower than the one estimated by fitting the thermal activation model to our data because of the temperature difference between the active volume of the sample and the Si substrate where it is measured. However, the temperature variation with current is similar in both cases. The parameters thus estimated, common to all models, are shown in table I. The effective thermal resistance, was found to be $R_{th} \approx 1.6 \times 10^4$ $K.W^{-1}$ a value compatible with previous work [24], with a variation of about 3% between the different models, while the activation energy $E_a = 0.269$ eV corresponds to the value obtained from the low current conductivity measured as a function of temperature [16].

All three models, as shown in Figure 5(a) give a very similar thermally induced variation of conductivity with current. All three reproduce the general variation in the experimental curve but show differences from it in the low current region.

The difference with respect to the experimental data in the low current region is probably due to the extended geometry of our structure leading to non-uniformity of the current and temperature in the effective NbO_2 volume. However, we find that the simpler thermal activation model gives results equivalent to the more complicated Poole-Frenkel models. This validates the correctness of the thermal activation phenomenon being at the root of the observed behavior, coupled with very low thermal conductivity. More complex phenomena (Poole Frenkel models) need to be invoked only when electric field effects are substantial

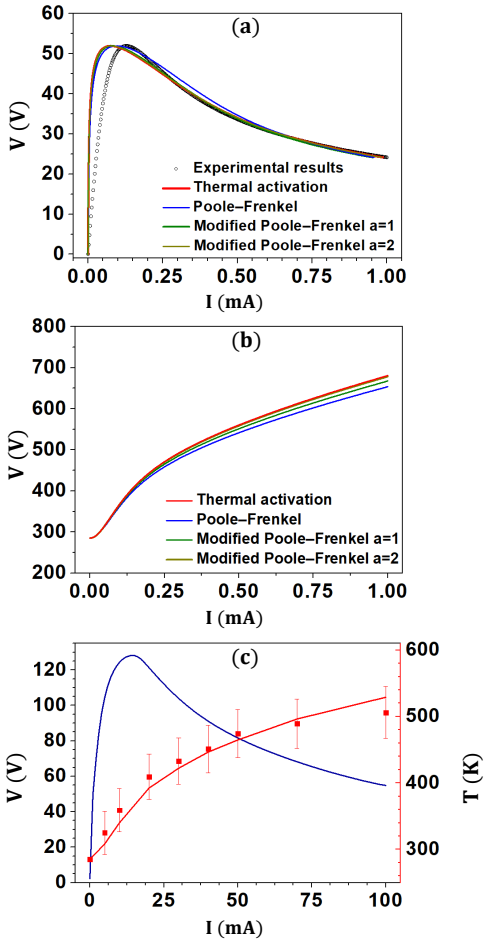

FIG. 5. Fits of the data by various transport models. (a) Measured and fitted $V(I)$ (b) Temperature variation as a function of current using Newton's law of cooling in the static limit. (c) Temperature variation as measured from the red-shift of the substrate Si Raman peak.

due to the nanometric size of devices.

In-situ Raman experiments at different regions of the NDR cycle and at different temperatures show that no electronic or structural phase change is observed in NbO_2 thin films in the NDR mode. In particular, even in the NDR domain where large changes in the resistivity occur, both crystalline and amorphous samples remain insulating since their resistance always decreases with increase in temperature. Eventual phase changes observed in literature may be due to the amorphous-crystalline change which occurs above 550°C. The metal insulator transition which occurs at about 800°C is probably never observed in such devices.

Temperature is the parameter which induces this change in resistivity through thermal activation of carriers. Temperature changes are locally induced because of power dissipated

by the current in the device and the intrinsically low thermal conductivity of NbO_2.

CONCLUSIONS

NDR in NbO_2 is caused by the variation of electrical conductivity by thermally generated charge carriers in a feedback loop phenomenon where the power dissipated by the device current determines local temperature. If the device is operated at a temperature where thermally generated charge carriers are sufficiently numerous, no NDR is observed. For amorphous NbO_2, this temperature is as low as 400 K and presumable about 100 K higher for crystalline NbO_2.

NDR is found in both amorphous and crystalline NbO_2 devices. However, the electrical conductivity of amorphous NbO_2 is more than that of crystalline NbO_2, which means that the I-V range where NDR is found is different in each material. The amorphous-crystalline transformation sets in above 550°C, while the Mott insulator-metal transition occurs at about 800°C. These transitions are not involved in the NDR phenomena in our devices. No phase transition, neither structural nor electronic and no irreversible phenomena could be related to NDR in our samples investigated using in-situ Raman spectroscopy.

Since NDR involves sizable variations of electrical conductivity generated by temperature change, it can be found in semiconductors or insulators where such sizable variation is possible through thermal energy. But for this to occur, considerable change in local temperature has to be possible through Joule heating. This implies low thermal conductivity in the material. Effectively, NbO_2 has a thermal conductivity which is two orders of magnitude lower than that of silicon and the electronic contribution to this thermal conductivity is negligible.

We acknowledge Ricardo Lobo for discussions. This work was supported by French state funds managed by the ANR within the Investissements d'Avenir programme under reference ANR-11-IDEX-0004-02, and more specifically within the framework of the Cluster of Excellence MATISSE led by Sorbonne Universités and from CEFIPRA grant 5908-2. The data required to reproduce these findings is available from the authors on request.

* johan.biscaras@sorbonne-universite.fr

† abhay.shukla@sorbonne-universite.fr

[1] D. V. Geppert, Proc. IEEE 51, 223 (1963).

[2] G. C. Vezzoli, S. Levy, B. Lalevic, and M. Shoga, J. Appl. Phys. **54**, 5828 (1983).

[3] J. Bae, I. Hwang, Y. Jeong, S. Kang, S. Hong, J. Son, J. Choi, J. Kim, J. Park, M.Seong, Q. Jia, and B. Ho Park, Appl. Phys. Lett. **100**, 062902 (2012).

[4] X. Liu, S. Sadaf, M. Son, J. Park, J. Shin, W. Lee, K. Seo, D. Lee, and H. Hwang, IEEE Electron Device Lett. **33**, 236 (2012).

[5] X. Liu, S. Sadaf, S. Park, S. Kim, E. Cha, D. Lee, G. Jung, and H. Hwang, IEEE Electron Device Lett. **34**, 235 (2013).

[6] M. Pickett, and R. Williams, Nanotechnology **23**, 215202 (2012).

[7] H. Philipp, and L. Levinson, J. Appl. Phys. **50**, 4814 (1979).

[8] S. Li, X. Liu, S. K. Nandi, D. Venkatachalam, R. Elliman, Proc. Optoelectron Microelectron Mater. Devices, Perth, WA, Australia, 138 (2014).

[9] Y. Wang, R. Comes, S. Wolf, and J. Lu, IEEE Journal of the Electron Devices Society **4**, 11 (2015).

[10] S. Shin, T. Halpern, and P. Raccah, J. Appl. Phys. **48**, 3150 (1977).

[11] S. Kumar, Z. Wang, N. Davila, N. Kumari, K. Norris, X. Huang, J. Strachan, D. Vine, A. Kilcoyne, Y. Nishi, and R. Williams, Nat. Commun. **8**, 658 (2017).

[12] T. Joshi, P. Borisov, and D. Lederman, J. Appl. Phys. **124**, 114502 (2018).

[13] Y. Wang, R. B. Comes, S. Kittiwatanakul, S. A. Wolf,and J. Lu, J. Vac. Sci. Technol. A **33**, 021516 (2015).

[14] Z. Wang, S. Kumar, R. Williams, Y. Nishi, and H. Wong, App. Phys. Lett., **114**, 183501 (2019).

[15] S. Kim, J. Park, J. Woo, C. Cho, W. Lee, J. Shin, G. Choi, S. Park, D. Lee, B. Hun Lee, and H. Hwang, Microelectronic Engineering, **107**, 33 (2013).

[16] A. Fakih, J. Biscaras, and A. Shukla, cond-mat/arXiv:1910.02824, http://arxiv.org/abs/1910.02824

[17] E. Santos, D. Freitas, I. Fier, J. Fernandes, M. Continentino, A. de Oliveira, and L. Walmsley,

J. of Phys. and Chem. of Solids **90**, 65 (2016).

[18] R. Ongaro, and A. Pillonnet, Revue de Physique Appliquee **24**, 1085 (1989).

[19] P. Rottlander, M. Hehn, and A. Schuhl, Phys. Rev. B **65**, 054422 (2002).

[20] J. L. Hartke, J. Appl. Phys. **39**, 4871 (1968).

[21] P. L. Young, J. Appl. Phys. **47**, 235 (1976).

[22] G. Gibson, S. Musunuru, J. Zhang, K. Vandenberghe, J. Lee, C. Hsieh, W. Jackson, Y. Jeon, D. Henze, Z. Li, and R. Williams, Appl. Phys. Lett. **108**, 023505 (2016).

[23] S. Slesazeck, H. Mahne, H. Wylezich, A. Wachowiak,a J. Radhakrishnan, A. Ascoli, R. Tetzlaffb, and T. Mikolajickab, Physical model of threshold switching in NbO_2 based memristors. RSC Adv. **5**, 102318 (2015).

[24] H. Cho, G. Kimb, T. Onozato, H. Jeenc, and H. Ohta, International Journal of Heat and Mass Transfer **137**, 263 (2019).